Effect of Surface Produced H$^-$ Ion on the Plasma Meniscus in Negative Hydrogen Ion Sources

Katsuya HAYASHI, Kazuo HOSHINO, Akiyoshi HATAYAMA,
Kenji MIYAMOTO[1)] and Jacques LETTRY[2)]

Keio University, Kanagawa 223-8522, Japan
[1)]*Naruto University of Education, Tokushima 772-8502, Japan*
[2)]*CERN Rte de Meyrin, 1200 Geneva, Switzerland*

(Received 18 July 2022 / Accepted 14 November 2022)

To extract intense ion beams with good beam optics from ion sources, controlling the distance d_{eff} between the plasma meniscus (i.e., beam emission surface) and the beam extraction grid is important. This study conducts a novel investigation into the dependence of the effective distance d_{eff} on the amount of surface H$^-$ production S_{H^-}. For this purpose, a 3D PIC (three dimensional Particle-in-Cell) simulation is conducted to obtain a model geometry of the extraction region for a H$^-$ ion source with S_{H^-} as a parameter. Based on results, d_{eff} significantly depends on S_{H^-} and the H$^-$-electron density ratio ($\alpha = n_{\mathrm{H}^-}/n_e$) in front of the extraction aperture for the same plasma density; as S_{H^-} increases, d_{eff} decreases. The results suggest that S_{H^-} is critical for controlling d_{eff} and the resultant beam optics extracted from the negative ion source.

Keywords: negative ion source, particle-in-cell, plasma meniscus, surface-produced ion

DOI: 10.1585/pfr.18.1401008

1. Introduction

Negative hydrogen ion (H$^-$) sources are utilized in a wide range of fields; for example, high energy particle physics [1,2], fusion plasma heating [3–6], and medical applications [7, 8]. Ideally, H$^-$ ion sources must produce high intensity beams with good convergence. To improve beam convergence, controlling the effective distance d_{eff} between the plasma meniscus (beam-ion emitting surface) and the extraction grid (EG) is important. In other words, the so-called perveance matching is indispensable for improving beam quality [9].

Figure 1 shows the schematic relationship between the plasma meniscus and EG. In Fig. 1, the gray region shows the region around the extraction aperture with plasma. Blue parallel lines represent the plasma grid (PG) and the EG. Based on the geometrical distance d between the PG and EG, d_{eff} is classified into the following three cases: i) $d_{\mathrm{eff}} = d$ (Fig. 1 (a)), ii) $d_{\mathrm{eff}} < d$ (Fig. 1 (b)), iii) $d_{\mathrm{eff}} > d$ (Fig. 1 (c)).

As seen from Fig. 1, controlling d_{eff} is important for improving beam convergence. In Fig. 1 (a), the plasma meniscus (beam-ion emitting surface) is flat, achieving perveance matching; moreover, the extracted beam has good quality. In Fig. 1 (b), the plasma meniscus is convex, resulting in a diverged extracted beam. The plasma meniscus is concave in Fig. 1 (c), resulting in an over-focused extracted beam, which then diverges.

For positive hydrogen (H$^+$) ion extraction in a positive ion source, d_{eff} is estimated as follows [10]:

$$d_{eff}^2 = \frac{4}{9e}\varepsilon_0 \sqrt{\frac{2e}{kT_e}} \frac{V^{\frac{3}{2}}}{n_{se}}, \tag{1}$$

where n_{se} is the H$^+$ ion density at the sheath edge and V is the extraction voltage between EG and PG. T_e is the electron temperature. In addition, e, ε_0, and k are the elementary charge, vacuum permittivity, and Boltzmann constant, respectively. Equation (1) is obtained by equating the current density j_s of the ion saturation current with the current density j_{ext} of space-charge limited extraction current, which are expressed as follows [9, 10]:

$$j_s = en_{se}\sqrt{\frac{kT_e}{M_i}}, \tag{2}$$

$$j_{ext} = \frac{4}{9}\varepsilon_0 \sqrt{\frac{2e}{M_i}} \frac{V^{\frac{3}{2}}}{d^2}, \tag{3}$$

where M_i is H$^+$ ion mass. In Eq. (1), the effective distance d_{eff} depends on the extraction voltage V, electron temperature T_e, and plasma density at the sheath edge n_{se} in the case of H$^+$ extraction from ordinary plasma without negative ions.

However, the parameter dependence of d_{eff} is still unclear in the case of highly efficient H$^-$ ion extraction, i.e., for a large number of surface-produced negative ions.

In ordinary plasma, electrons reach the wall earlier than positive ions due to their mass difference. Consequently, the electric potential of the wall is lower than that of the plasma. Accordingly, the sheath forms if the positive ions fulfill Bohm criterion.

author's e-mail: phy-kh@keio.jp

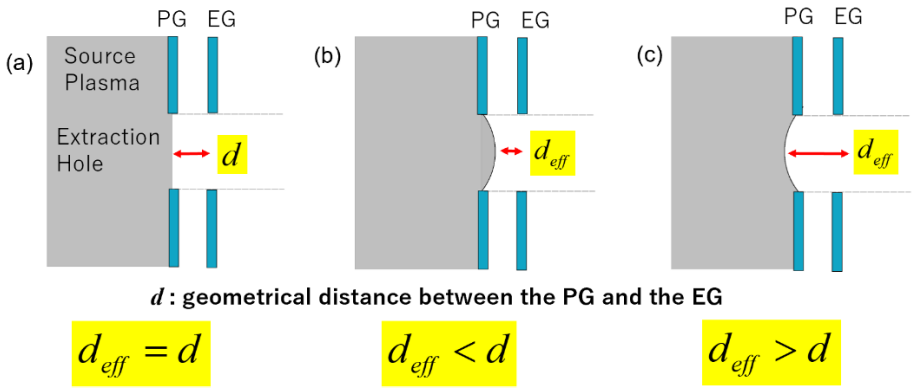

Fig. 1 Geometrical distance d is the distance between the PG and EG. The effective distance d_{eff} is defined as the distance between the plasma meniscus (beam-ion emitting surface) and the EG.

However, for plasma with a large number of surface-produced negative ions that are much heavier than electrons, the aforementioned mechanism is not necessarily applicable to the formation of the positive ion sheath. Recently, ion-ion plasma, which consists of only H^+ ions and H^- ions without electrons, has been reportedly observed near the extraction aperture [11]. The effective distance d_{eff} and its parameter dependence are still unclear, especially in cases with a large number of H^- ions near the extraction aperture.

This paper aims to clarify the effect of the amount of surface-produced H^- ions $S_{\mathrm{H^-}}$ on the effective distance d_{eff} for H^- extraction, with a focus on studying d_{eff} under the case of a large number of H^- ions being produced at the PG surface. For this purpose, three dimensional Particle-in-Cell (3D PIC) simulations are conducted. In these simulations, only $S_{\mathrm{H^-}}$ is changed and other parameters are fixed, i.e., n_{se}, V, and T_e are maintained almost constant. The model is described in Sec. 2. The results of the effects of $S_{\mathrm{H^-}}$ on d_{eff} in 3D PIC simulations are detailed in Sec. 3. In Sec. 4 the conclusion is summarized, and future work is discussed.

2. Simulation Model

A 3D PIC code (Keio-BFX) is used to study the effect of $S_{\mathrm{H^-}}$ on d_{eff}. Detailed explanations of the Keio-BFX code have already been reported [12–14]. Herein, the model used in the present study is briefly summarized using the Keio-BFX code.

The motion of H^+ ions, electrons, and H^- ions is determined by the following equations of motion:

$$\frac{\mathrm{d}\boldsymbol{x}}{\mathrm{d}t} = \boldsymbol{v}, \quad \frac{\mathrm{d}\boldsymbol{v}}{\mathrm{d}t} = \frac{q}{m}(\boldsymbol{E} + \boldsymbol{v} \times \boldsymbol{B}), \tag{4}$$

where $\boldsymbol{x}$, $\boldsymbol{v}$, q, and m are the position, velocity, charge, and mass of a particle. Furthermore, $\boldsymbol{E}$ and $\boldsymbol{B}$ are the electric and magnetic field at the particle position. The equation of motion is discretized using the Buneman-Boris Leapfrog method [15].

$$\frac{\boldsymbol{x}_{k+\frac{1}{2}} - \boldsymbol{x}_{k-\frac{1}{2}}}{\Delta t} = \boldsymbol{v}_k, \tag{5}$$

$$\frac{\boldsymbol{v}_{k+1} - \boldsymbol{v}_k}{\Delta t} = \frac{q}{m}\left(\boldsymbol{E}_{k+\frac{1}{2}} + \frac{\boldsymbol{v}_k + \boldsymbol{v}_{k+1}}{2} \times \boldsymbol{B}_{k+\frac{1}{2}}\right), \tag{6}$$

where the subscript k $(= 0, 1, 2 \ldots)$ denotes the time step of the Leapfrog method.

The electric field in Eq. (4) is solved using the Poisson equation in a self-consistent manner with the particle motion, as follows:

$$\nabla^2 \varphi = -\frac{\rho}{\varepsilon_0}, \tag{7}$$

where φ is the electric potential, and ρ is the charge density. The electric field is given by $\boldsymbol{E} = -\nabla\varphi$. Charge density ρ is calculated from the particle positions obtained using the aforementioned equations of motion (Eq. (4)). Poisson equation (Eq. (7)) is numerically solved using the Bi-Conjugate Gradient Stabilized Method to compute the electric potential at each mesh point using the Algebraic MultiGrid method as a preconditioner [16, 17].

Figure 2 shows the model geometry used in this study. It is the same model geometry as that in Ref. [14] for the extraction region of the Linac4 ion source [1, 2]. The simulation domain is 3D, and the initial plasma is generated inside a cylindrical source on the left side of Fig. 3. The z-axis is along the direction of the negative ion beam extraction.

As shown in Fig. 3, Dirichlet boundary conditions are used for the PG surface as well as the inner wall of the plasma chamber, where the potential is set as zero. To set the boundary condition on the right-hand side boundary (EG-side boundary) of the simulation domain in Fig. 3, the potential values $V_{\mathrm{EG\text{-}S}}$ are calculated for a given EG voltage V_{EG} (7 kV) on the EG of the Linac4 ion extraction system under the vacuum condition prior to the present 3D PIC simulations. Next, Dirichlet boundary conditions are used on the EG-side boundary. In addition, the boundary conditions for the particles reaching the simulation boundaries

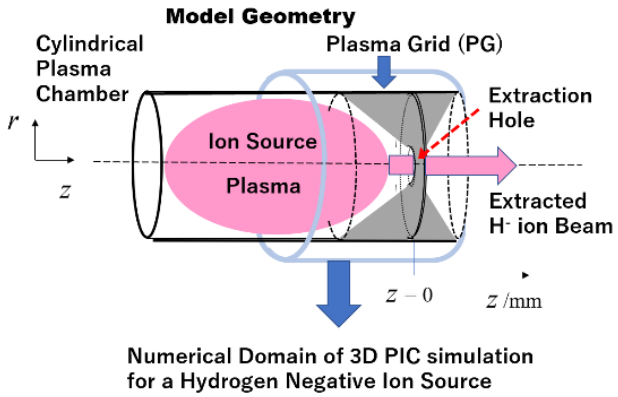

Fig. 2 Model geometry in the simulation.

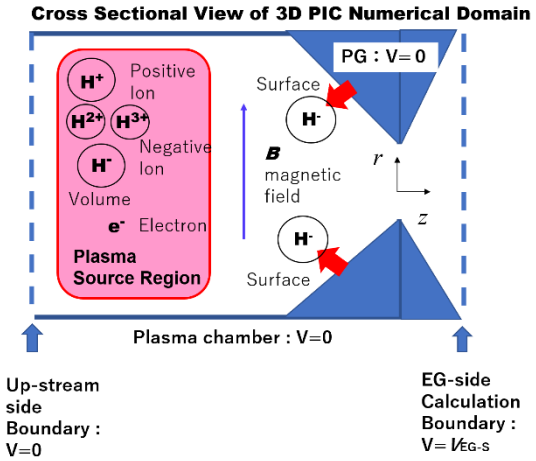

Fig. 3 Cross-sectional view of 3D PIC numerical domain along with the initial loading of particles and boundary condition imposed on each boundary to solve Poisson equation.

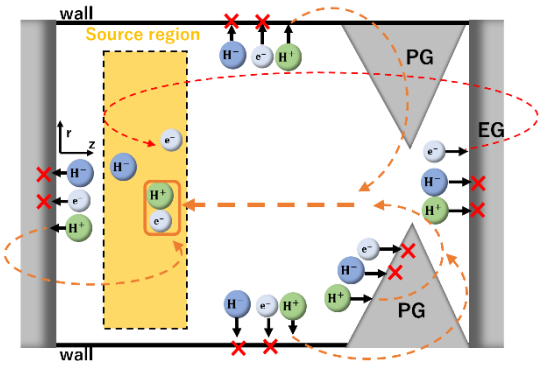

Fig. 4 Boundary conditions imposed on the particles in the 3D PIC simulation. The condition depends on particle species and the boundary where each particle crosses.

are the same as those in Ref. [14] and are schematically shown in Fig. 4.

The magnetic field profile is also the same as in Ref. [14]. The profiles for the strength of the magnetic field $\boldsymbol{B}$ are shown in Fig. 5 and Fig. 6. Figure 5 shows the 2D profile in the y-z plane, while Fig. 6 shows the 1D profile along the extraction axis (z-axis). As seen from these figures, the magnetic field strength is approximately in the range of 12 - 18 mT in the upstream region of the extraction aperture and the direction is perpendicular to the extraction axis (z-axis).

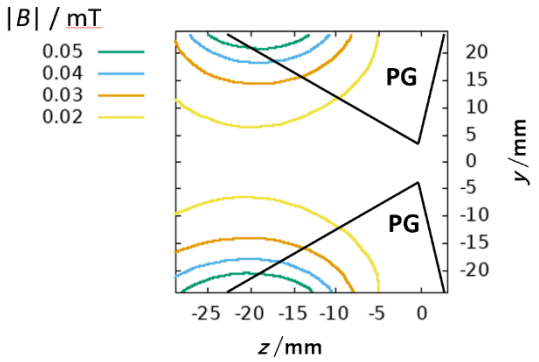

Fig. 5 Magnet field strength in the y-z plane.

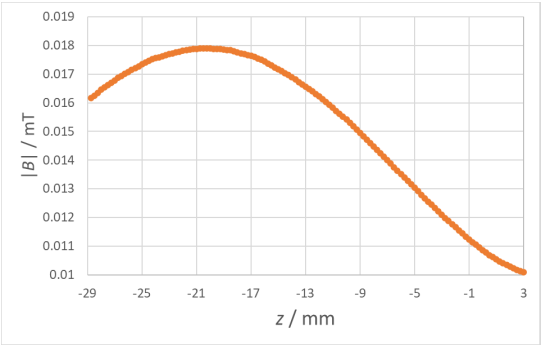

Fig. 6 Magnet field strength along the extraction axis (z-axis) of the simulation domain.

Table 1 lists the parameters used to define the simulation domain and the mesh used in the PIC model. These parameters are based on the results obtained from simulations using the NINJA code [18, 19]. They are almost the same as those in Ref. [14] except for the surface H^- production. The simulations in Ref. [14] only consider the volume H^- production. In contrast, this study considers the surface-produced H^- ions. The current density of surface-produced H^- ions from the PG is provided as a fixed parameter for simplicity. In this study, small surface production case (Case A) and large one (Case B) are simulated with current densities of 1168 A/m^2 and 2336 A/m^2, respectively.

A direct and precise evaluation of S_{H^-} in experiments is difficult because of many unknown factors (e.g., Cs coverage, wall surface temperature, and neutral fluxes). Herein, following Ref. [20], the values of S_{H-} for Cases A and B are specified in Table 1. These values are considered as reasonable, at least the orders of magnitude of these values are not significantly different from the values in typical experiments with a large number of surface-produced

Table 1 Plasma and PIC parameters.

Parameter	**Value**
Electron density	1.0×10^{18} m^{-3}
Electron temperature	3.6 eV
Positive and negative ions temperature	1.6 eV
Density ratio of initial plasma ($n_e : n_{H^+} : n_{H_2^+} : n_{H_3^+} : n_{H^-}$)	0.985 : 0.740 : 0.074 : 0.186 : 0.015
Debye length (λ_{De})	1.41×10^{-5} m
Electron thermal velocity	7.96×10^{5} m/s
Plasma frequency (ω_p)	5.64×10^{10} rad/s
Surface production rate S_{H^-}	Case A: 1168 A/m^2; Case B: 2336 A/m^2
Extraction voltage	7 kV
Real size	$48 \times 48 \times 31.75$ mm^3
Scaling factor	3.5×10^{-2}
Number of superparticles	2 500 000
Number of Numerical Mesh in the x, y, z directions	$196 \times 196 \times 128$
Mesh size	$0.625\lambda_{De}$
Time step	$0.4/\omega_p = 7.09 \times 10^{-12}$ s
Simulation time	100 000 time steps = 0.7 μs
Magnetic field strength	10∼18 mT

H^- ions from Cs-seeding.

Surface production is simulated as described next. First, the location of the starting point is uniformly chosen on the PG surface using uniform random number. Second, the angular distributions of the polar angle θ and the rotation angle φ with respect to the normal of the PG surface are sampled from a cosine distribution and uniform distribution, respectively. Finally, the velocities of surface-produced H^- ions are selected from the Maxwell distribution with an average energy of 1.6 eV using the Box–Muller method.

The following reaction processes in the plasma volume are considered using the null collision method [21]: i) H^- production DA (Dissociative Attachment: $e + H_2 \rightarrow H^- + H$); and ii) H^- destruction process by neutral atom AD (Associative Detachment: $H^- + H \rightarrow H + H + e$ and $H^- + H \rightarrow H_2 + e$) [22]. A more systematic approach on collision species and their cross section data is an avenue for future research as discussed in Sec. 4.

In the present simulation, the reduced-size-scaling approach with a scaling factor ($s = 3.5 \times 10^{-2}$) is adopted to save on the computational cost by setting important normalized parameters ρ_j^* ($= r_{Lj}/L$) and λ_{jk}^* ($= \lambda_{jk}/L$) the same as those in the real system. Note that L is the characteristic scale length of the real system, while r_{Lj} and λ_{jk} are the Larmor radius and collision mean free path, respectively. The symbols j and k denote particle species. To study the basic characteristics of low-density and low-temperature plasmas close to the wall including the thin sheath region in large scale devices, the reduced-size-scaling approach is very useful and effective for PIC modeling because the calculation cost for PIC simulations is significant, especially for 2D and 3D PIC modeling. This idea of setting the important normalized parameters in a numerical simulation model the same as those in the corresponding real system is similar to the similarity rule in fluid dynamics. The reduced-size scaling has been already used for various PIC simulations; for example, the Scrape-off Layer and divertor plasmas in large fusion tokamak devices [23] as well as the H^- ion source plasmas [24–28].

To set ρ_j^* and λ_{jk}^* in the present simulations of H^- ion extraction the same as in the real system, the magnetic field and the collision mean free path are scaled as $B_{sim} = s^{-1}B$ and $\lambda_{sim} = s\lambda_{jk}$, respectively, while the system length following the reduced-size scaling is given by $L_{sim} = sL$. Note that the normalized Debye length λ_D/L_{sim} (L_{sim} is the scale length of the simulation model) becomes larger than in the real system after implementing the reduced-size scaling. However, the sheath property limitedly depends on the value of λ_D/L_{sim}, if λ_D/L_{sim} in the simulation is set small enough ($\lambda_D/L_{sim} < 10^{-2} - 10^{-3}$), at least for a simple 1D problem. This has been confirmed by the kinetic study in Ref. [29] by numerically solving the plasma-sheath equation derived by the Vlasov equation and Poisson equation.

As mentioned earlier, various studies [24–28] have adopted the same type of PIC model as the present model with the reduced-size scaling to understand the H^- ion extraction process. The simulation results and effectiveness of the reduced-size-scaling approach are verified step-by-step through model validation by comparing with various experiments and other theoretical results [20, 30]. The proposed model gives useful insights into the H^- extraction process as well as effectively identifies basic and intrinsic mechanisms of various interesting phenomena at the least in a qualitative manner.

3. Results

At the initial time step ($t = 0$), plasma particles are loaded at a random position inside the source region with the mixing ratio listed in Table 1 ($n_e : n_{H^+} : n_{H_2^+} : n_{H_3^+} : n_{H^-} = 0.985 : 0.740 : 0.074 : 0.186 : 0.015$). After that ($t > 0$), the boundary conditions shown in Fig. 4 are imposed on the particles crossing each boundary at each time step. With the boundary conditions shown in Fig. 4, a quasi-steady state is obtained for each case after approximately 100000 time steps. Figure 7 shows the time evolution of the total number of particles for each particle species in Case A. To obtain a reasonable statistical accuracy, the time average of the plasma parameters and potential is evaluated over 2500 time steps after reaching a quasi-steady state.

At first, the formation of ion-ion plasma is verified as in the experiments with a large number of surface-produced H^- ions. Figure 8 shows the spatial profile of the density ratio of H^- ions to electrons ($\alpha = n_{H^-}/n_e$) along the extraction axis (z-axis). In this paper, $\tilde{z}$ represents the cell number. The positions $\tilde{z} = 0$ and $\tilde{z} = 128$ correspond to the left- and right-hand side boundaries, respectively. Blue and red dots represent the α values for Cases A and B, respectively. This result showcases that the proposed simulation model successfully reproduces ion-ion plasma with $\alpha > 20$ for both Cases A and B with reasonable S_{H^-} surface flux.

Figure 9 shows the 2D profile of electric potential near the extraction aperture in the y-z plane. The left and right sides showcase the profiles for Cases A and B, respectively. The red contour marks the plasma potential of 1.5 V. Herein, plasma potential is defined as $\Delta\varphi_{s_w} = \varphi_s - \varphi_w$ between the two typical points, namely, $\varphi_s = 1.5$ V at the edge of source region and $\varphi_w = 0$ V at the wall. This value is smaller than the following theoretical value of $\Delta\varphi_{th}$ predicted by the general sheath theory for ordinary plasma comprising only positive ions and electrons without negative ions [31, 32]:

$$\Delta\varphi_{th} = \frac{1}{2}\frac{kT_e}{e}\ln\left(\frac{1}{2\pi}\frac{m_i}{m_e}\right).$$

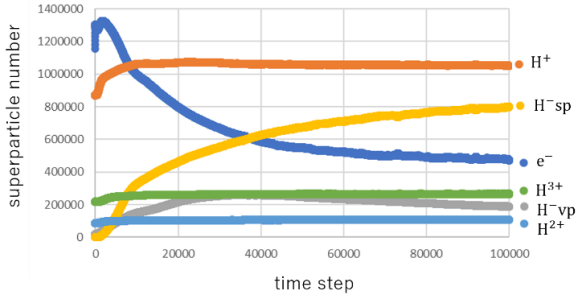

Fig. 7 Time evolution of the total number N_j of the j-th particle species ($j = e^-$, H^+, H^-vp, H^-sp, H^{2+}, and H^{3+}, where H^-vp and H^-sp represent the volume and surface-produced H^- ions, respectively).

For hydrogen plasma with only positive ions and electrons, $\Delta\varphi_{th}$ is

$$\Delta\varphi_{th} \sim 3\frac{kT_e}{e} = 10.8\,\text{eV},$$

with $T_e = 3.6$ eV used in the present 3D PIC simulation. However, in this simulation, a large number of negative ions exist in the plasma region, which are significantly heavier than electrons. Furthermore, the loss of H^- ions from the plasma region is less than that of electrons. In other words, H^- ions easily stay with H^+ ions in the plasma region to maintain quasi-neutrality. Therefore, the plasma potential for plasma with a large number of negative ions is smaller than that for ordinary plasma without negative ions.

As seen from the comparison of the two potential profiles, the extraction voltage penetrates more deeply into the ion source region for Case A than that for Case B. This result implies that the effective distance d_{eff} increases due to decreasing S_{H^-}.

To discuss d_{eff} more quantitatively, the position of the plasma meniscus must be defined. As mentioned in Sec. 1, for the case of positive (H^+) ion extraction from ordinary plasmas without negative (H^-) ions, d_{eff} is estimated by equating the ion saturation current at the sheath edge to the space-charge-limited extraction current. This means that the sheath edge is defined as the plasma meniscus for H^+ extraction.

This definition is based on the following idea: In the plasma region, plasma quasi-neutrality ($n_i \approx n_e$) holds and the electric field is approximately zero, i.e., $E = -d\varphi/dz \approx 0$. However, at the sheath boundary, electric potential starts decreasing towards the wall. Therefore, the position of plasma meniscus may be defined as the boundary where the electric potential starts decreasing as $d\varphi/dz < 0$ from $d\varphi/dz \approx 0$ (Definition I). Definition II is discussed later.

In contrast, for negative (H^-) ion extraction, the polarity of extraction voltage is not negative but positive. Therefore, with reference to Definition I for positive (H^+) ion ex-

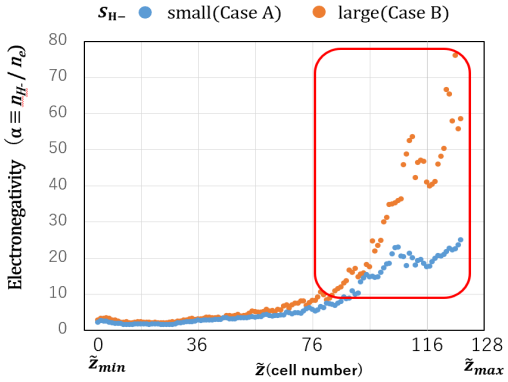

Fig. 8 Spatial profile of the density ratio of H^- ions to electrons $\alpha(= n_{H^-}/n_e)$; $\tilde{z}_{min}$ and $\tilde{z}_{max}$ correspond to $z = -28.75$ mm and $z = 3$ mm, respectively.

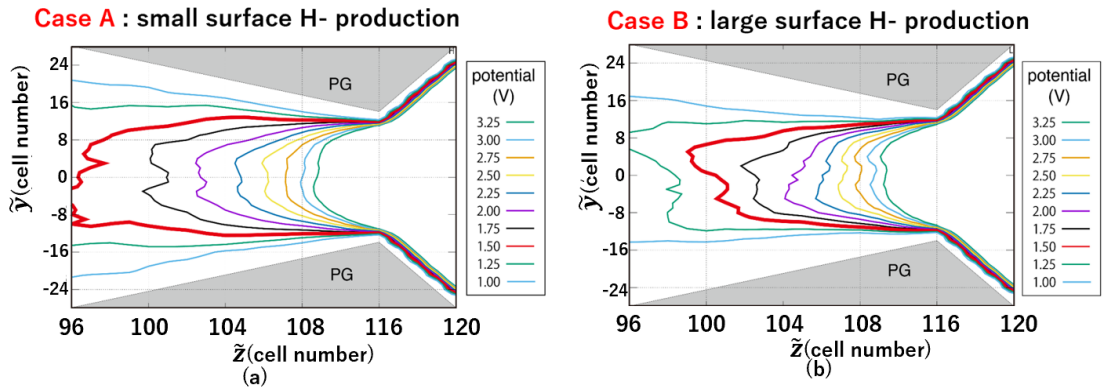

Fig. 9 Comparison of the 2D profiles of potential near the extraction aperture; $\tilde{z} = 96$ and $\tilde{z} = 120$ correspond to $z = -4$ mm and $z = 1$ mm in the real geometry, respectively.

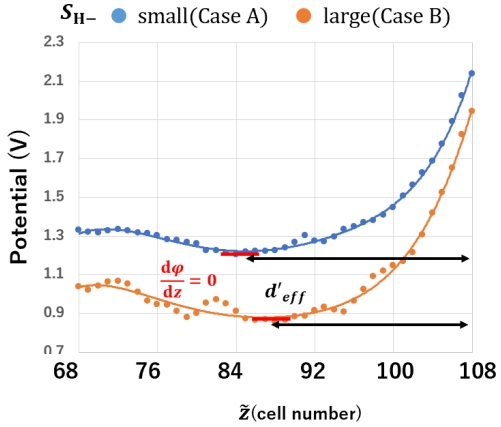

Fig. 10 Potential profile along the extraction z-axis ($\tilde{z} = 68$ and $\tilde{z} = 108$ correspond to $z = -11$ mm and $z = -1$ mm in the real geometry, respectively).

traction, plasma meniscus may be defined as the boundary where the electric potential starts increasing as $d\varphi/dz > 0$ from $d\varphi/dz \approx 0$ for the case of negative (H^-) ion extraction.

According to the aforementioned Definition I, plasma meniscus can be defined to evaluate the resultant $d_{\rm eff}$. Accordingly, the potential profile along the extraction axis (z-axis) has been plotted in Fig. 10. Blue and red dots represent the potential profile for Cases A and B, respectively. The blue and orange lines are obtained by polynomial approximation of the corresponding potential profiles. For Case B, the potential starts increasing closer to the EG (the right-hand side boundary). The effective distance $d_{\rm eff}$ is smaller for Case B than that for Case A.

In Fig. 10, plasma meniscus is defined by the potential profile based on Definition I. Plasma meniscus may also be defined in a different way using the density profile (Definition II). Whether the dependence of $d_{\rm eff}$ on $S_{\rm H^-}$ changes by changing the definition of plasma meniscus must be verified.

Before describing Definition II for H^- extraction in detail, first the potential profile and the resultant density profile near the extraction aperture are discussed for H^+ extraction. The electric potential starts decreasing towards the wall at the sheath boundary for H^+ extraction. Due to this potential drop towards the wall and extraction aperture, bulk electrons are reflected in the sheath region back to the plasma region. Therefore, the electron density in the sheath region is considerably smaller than the ion density, and only positive ions exist primarily ($n_{\rm H+} \gg n_e$). According to the sheath theory [31, 32], the electron density becomes about half of bulk plasma density ($n_e \sim 0.5 n_p$) even at the sheath entrance and further decreases rapidly closer to the wall in the sheath region with a significantly thin layer (several Debye-lengths). Based on the aforementioned physical background, the position of plasma meniscus may be defined as the boundary where the electron density is considerably smaller than the plasma density n_p in the bulk plasma ($n_p \gg n_e$).

In contrast to H^+ extraction, the polarity of the extraction voltage $V_{\rm EG}$ is reversed for H^- extraction. More specifically, a negative extraction voltage ($V_{\rm EG} < 0$) is applied to the EG with respect to the grounded PG ($V = 0$) for H^+ ion extraction, while a positive extraction voltage ($V_{\rm EG} > 0$) is applied to the EG for H^- ion extraction. Due to this difference in the polarity of the extraction voltage $V_{\rm EG}$, not electrons, but positive ions are reflected by the positive extraction voltage near the extraction aperture for H^- extraction. To understand the difference more clearly, a comparison of the electric potential profiles along the extraction axis is schematically shown in Fig. 11. In addition, the resultant particle dynamics for each species are shown in Fig. 11, not only in the region between the PG and EG, but also in the region close to the PG inside the ion source.

As seen from Fig. 11, for H^+ extraction, electrons are reflected at the point where all their initial kinetic energy is consumed by the potential drop. However, for H^- extraction, H^+ ions are reflected at the point where all their initial kinetic energy is consumed by the potential increase. Only a few ions with significantly high kinetic energy/velocity, enough to overcome the potential increase, can move further towards the outside of the ion source throughout the

extraction aperture. Consequently, H^+ ion density significantly decreases towards the extraction aperture.

Based on the aforementioned physical background, the plasma meniscus (the plasma boundary) may be defined (Definition II) as the boundary where the H^+ ion density becomes considerably smaller than the bulk plasma density ($n_p \gg n_{H+}$). H^- ions start being extracted near this low H^+ ion density region. As already shown in Fig. 10, note that the numerical result of the potential profile along the extraction axis is approximately the same as the schematic drawing shown in Fig. 11 (b); moreover, its polarity is clearly opposite to the one for H^+ extraction in Fig. 11 (a).

Figure 12 shows the 2D density profiles of H^+ ions around the extraction aperture. Figures 12 (a) and (b) correspond to those for Cases A and B, respectively. To apply Definition II in this case, the H^+ ion density that defines the plasma meniscus and $d_{\rm eff}$ must be specified. In the present study, a specific value of the ion density $n_{H+} = 10^{17}$ m^{-3} is used, which is smaller than the sheath edge density $n_{se} = 0.5n_p \sim 5 \times 10^{17}$m^{-3} ($n_p$ is the plasma density in the quasi-neutral region, $n_p \sim 10^{18}$m^{-3}) [31, 32]. Comparing Figs. 12 (a) and (b), $d_{\rm eff}$ and $S_{\rm H^-}$ are clearly inversely proportional to each other.

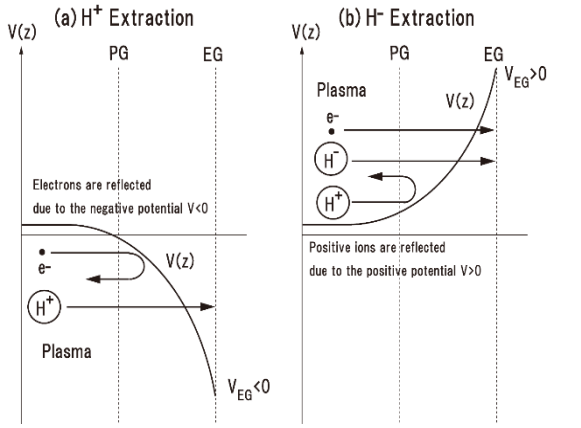

Fig. 11 Electric potential profiles along the extraction axis and resultant particle dynamics are compared between (a) H^+ extraction and (b) H^- extraction.

Figure 13 shows a comparison of the H^+ ion density profiles along the extraction axis between Cases A and B. Note that the H^+ ion density starts decreasing near the extraction aperture. In addition, the starting point of the density decrease is more on the inside (smaller z) for Case A than that for Case B. This means that the plasma meniscus for Case A is located more inside the source than that for Case B, i.e., $d_{\rm eff}$ for case A is larger than that for Case B.

The effective distance $d_{\rm eff}$ in Fig. 10 and Fig. 12 (Fig. 13) is obtained by using two different definitions of the plasma meniscus, namely, Definition I and Definition II, respectively. The effective distance $d_{\rm eff}$ derived from both definitions has the same tendency, i.e., $d_{\rm eff}$ becomes smaller for larger $S_{\rm H^-}$, while $d_{\rm eff}$ becomes larger for smaller $S_{\rm H^-}$. In other words, this tendency is unchanged in either definition. Thus, this conclusion is reliable. Furthermore, comparing this $d_{\rm eff}$ tendency with the α profile in Fig. 8, note that $d_{\rm eff}$ becomes smaller for the case with higher values of α, while $d_{\rm eff}$ becomes larger for the case with lower values of α in front of extraction aperture. Therefore, $d_{\rm eff}$ diminishes in the ion-ion plasma with a high α. This is due to the larger space charge effect of H^- ions in comparison with electrons. The electric field produced by the negatively charged particles can prevent the penetration of the electric field for extraction into the source plasma. This may be the space charge effect. The mass of H^- ions is significantly larger than that of electrons; consequently, the residence time around the plasma meniscus is longer for H^- ions than that for electrons. Thus, the space charge effect may be more pronounced for H^- ions than that for electrons.

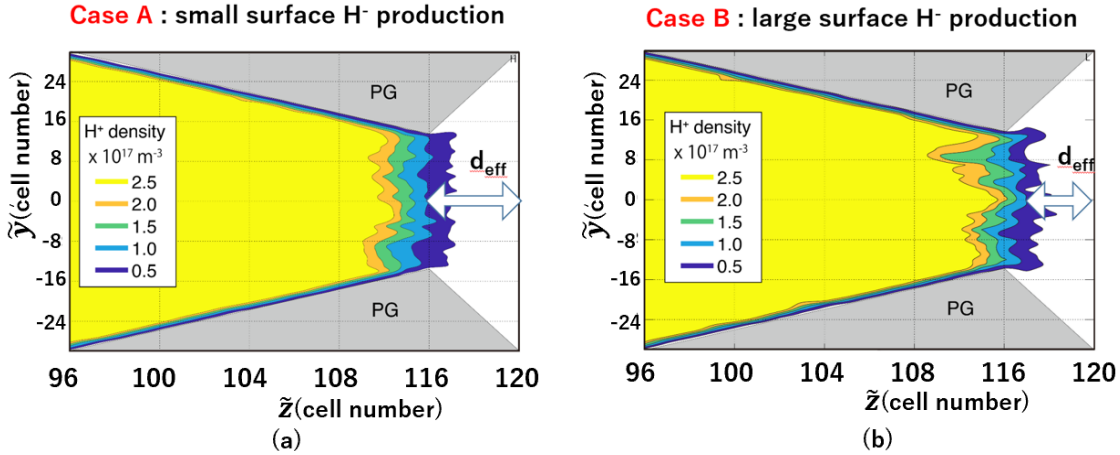

Fig. 12 Comparison of n_{H+} density profile and plasma meniscus ($\tilde{z} = 68$ and $\tilde{z} = 108$ correspond to $z = -11$ mm and $z = -1$ mm in the real geometry, respectively).

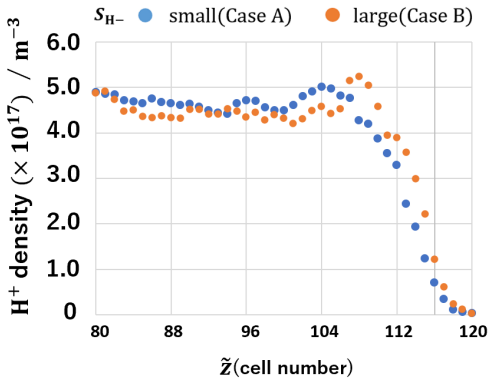

Fig. 13 1D profiles of the H+ ion densities along the extraction axis (z-axis) close to the extraction aperture ($\tilde{z} = 80$ and $\tilde{z} = 120$ correspond to $z = -9$ mm and $z = 1$ mm in the real geometry, respectively).

4. Summary and Future Problems

This study conducts a novel investigation into the effects of the amount of surface-produced H^- ions S_{H^-} on the effective distance $d_{\rm eff}$ using the Keio-BFX 3D PIC code along with the model geometry for the Linac4 ion source. In these simulations, only S_{H^-} is changed and the other parameters are fixed.

The dependence of $d_{\rm eff}$ on S_{H^-} is studied using the following two definitions of the position of plasma meniscus:

Definition I: the boundary where the electric potential starts increasing as $d\varphi/dz > 0$ from $d\varphi/dz \approx 0$.

Definition II: the boundary where the positive ion density becomes considerably smaller than the bulk plasma density ($n_{H+} = 10^{17}$ m^{-3} contour line).

Ion-ion plasmas with significantly large H^--electron density ratio $\alpha(= n_{H^-}/n_e) > 20$ have been reproduced for large S_{H^-} in the 3D PIC simulation as in the recent experiments.

The effective distance $d_{\rm eff}$ is demonstrated to depend on S_{H^-} and α $(= n_{H^-}/n_e)$ in front of the extraction aperture under the same plasma density. As S_{H^-} increases, $d_{\rm eff}$ decreases, while $d_{\rm eff}$ increases with decreasing S_{H^-}.

The results of this study suggest that S_{H^-} is crucial for controlling $d_{\rm eff}$ and the resultant beam optics extracted from the negative ion source.

In the present study, the effect ofS_{H^-} on $d_{\rm eff}$ is investigated and other parameters are fixed, i.e., n_{se}, V, and T_e are maintained almost constant. In the case that these parameters are changed, the effect of S_{H^-} on $d_{\rm eff}$ is unclear. Therefore, a more systematic investigation of the effect of S_{H^-} on $d_{\rm eff}$ while considering the changes in the aforementioned parameters is a scope for future study.

As described in Sec. 2, only the H^- production and H^- destruction processes in the volume are considered in this first study. In the future, more detailed collision processes/species will be considered for a more systematic analysis of the effects of collisions. To elaborate, as pointed out in Ref. [13], the Coulomb collision between a surface-produced H^- ion and H^+ ion in the plasma is critical with regards to velocity reversal and the resultant H^- density profile around the extraction aperture. The surface-produced H^- ions originally penetrate towards the center of the ion source from the PG. Therefore, the velocity reversal towards the extraction aperture is indispensable for effective H^- extraction. In addition, elastic collisions with neutral molecules and atoms could significantly affect the case of high neutral gas pressure, which can be applied to this study as well.

[1] J. Lettry *et al.*, Rev. Sci. Instrum. **85**, 02B122 (2014).
[2] J. Lettry *et al.*, Rev. Sci. Instrum. **87**, 02B139 (2016).
[3] R. Hemsworth *et al.*, Nucl. Fusion **49**, 045006 (2009).
[4] M. Kashiwagi *et al.*, Rev. Sci. Instrum. **83**, 02B119 (2012).
[5] K. Tsumori *et al.*, Rev. Sci. Instrum. **87**, 02B936 (2016).
[6] U. Fantz *et al.*, Rev. Sci. Instrum. **87**, 02B307 (2016).
[7] H. Etoh *et al.*, AIP Conf. Proc. **1869**, 030050 (2017).
[8] M. Onai *et al.*, AIP Conf. Proc. **1869**, 030043 (2017).
[9] S. Humphries Jr., *Charged Particle Beams*, Chap. 7, (John Wiley & Sons, New York, 1990).
[10] H. Zhang, *Ion Sources*, (Springer, Berlin, 1999).
[11] K. Tsumori *et al.*, AIP Conf. Proc. **1869**, 030001 (2017).
[12] S. Nishioka *et al.*, J. Appl. Phys. **119**, 023302 (2016).
[13] S. Nishioka *et al.*, J. Appl. Phys. **123**, 063302 (2018).
[14] M. Lindqvist *et al.*, J. Appl. Phys. **126**, 123303 (2019).
[15] C.K. Birdsall *et al.*, *Plasma Physics Via Computer Simulation*, (McGraw-Hill, 1991), pp. 58-63.
[16] H. van der Vorst, SIAM J. Sci. Stat. Comput. **13**, 631 (1992).
[17] K. Stuben, J. Comput. Appl. Math. **128**, 281 (2001).
[18] S. Mattei *et al.*, J. Comp. Phys. **350**, 891 (2017).
[19] S. Briefi *et al.*, New J. Phys. **19**, 105006 (2017).
[20] R. McAdams *et al.*, Plasma Sources Sci. Technol. **20**, 035023 (2011).
[21] R.K. Janev *et al.*, *Elementary Processes in Hydrogen-Helium Plasmas: Cross Sections and Reaction Rate Coefficients,* (Springer, Berlin, 1987).
[22] R.W. Hockney and J.W. Eastwood, *Computer Simulation Using Particles*, Chap. 9, IOP publishing, (Bristol, UK, 1988).
[23] T. Takizuka *et al.*, Nucl. Fusion **49**, 075038 (2009).
[24] K. Miyamoto *et al.*, Appl. Phys. Lett. **100**, 233507 (2012).
[25] K. Miyamoto *et al.*, Appl. Phys. Lett. **102**, 023512 (2013).
[26] A. Hatayama, Rev. Sci. Instrum. **79**, 02B901 (2008).
[27] S. Kuppel *et al.*, J. Appl. Phys. **109**, 013305 (2011).
[28] A. Hatayama *et al.*, New J. Phys. **20**, 065001 (2018).
[29] G.A. Emmert *et al.*, Phys. Fluids **23**, 803 (1980).
[30] A. Fukano and A. Hatayama, AIP Conf. Proc. **1390**, 68 (2011).
[31] P.C. Stangeby, *The Plasma Boundary of Magnetic Fusion Devices*, Chap. 2, University of Toronto Institute for Aerospace Studies.
[32] P.C. Stangeby, *The Plasma Sheath*, in NATO ASI series, Series B, *Physics of Plasma-Wall interactions in Controlled Fusion*, edited by D. E. Post and R. Behrish, (Plenum Press, New York, 1986), pp. 41-97.